

Electron vs Energy Transfer in Arrays Featuring Two Bodipy Chromophores Axially Bound to a Sn(IV) Porphyrin via a Phenolate or Benzoate Bridge

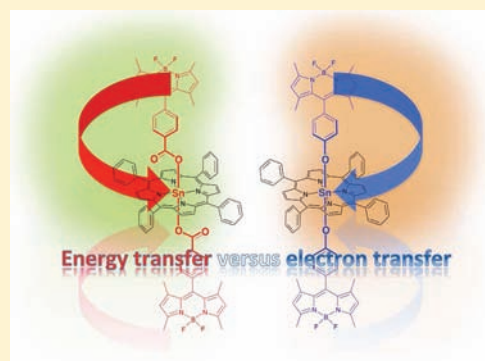
Theodore Lazarides,[†] Susanne Kuhri,[‡] Georgios Charalambidis,[†] Manas K. Panda,[†] Dirk M. Guldi,^{*,‡} and Athanassios G. Coutsolelos^{*,†}

[†]Chemistry Department, University of Crete, Voutes Campus, P.O. Box 2208, 71003 Heraklion, Crete, Greece

[‡]Department of Chemistry and Pharmacy, Interdisciplinary Center for Molecular Materials (ICMM), Friedrich-Alexander-Universitaet Erlangen-Nuernberg, Egerlandstrasse 3 91058 Erlangen, Germany

Supporting Information

ABSTRACT: In this report we describe the synthesis of multichromophore arrays consisting of two Bodipy units axially bound to a Sn(IV) porphyrin center either via a phenolate (**3**) or via a carboxylate (**6**) functionality. Absorption spectra and electrochemical studies show that the Bodipy and porphyrin chromophores interact weakly in the ground state. However, steady-state emission and excitation spectra at room temperature reveal that fluorescence from both the Bodipy and the porphyrin of **3** are strongly quenched suggesting that, in the excited state, energy and/or electron transfer might occur. Indeed, as transient absorption experiments show, selective excitation of Bodipy in **3** results in a rapid decay ($\tau \approx 2$ ps) of the Bodipy-based singlet excited state and a concomitant rise of a charge-separated state evolving from the porphyrin-based singlet excited state. In contrast, room-temperature emission studies on **6** show strong quenching of the Bodipy-based fluorescence leading to sensitized emission from the porphyrin moiety due to a transduction of the singlet excited state energy from Bodipy to the porphyrin. Emission experiments at 77 K in frozen toluene reveal that the room-temperature electron transfer pathway observed in **3** is suppressed. Instead, Bodipy excitation in **3** and **6** results in population of the first singlet excited state of the porphyrin chromophore. Subsequently, intersystem crossing leads to the porphyrin-based triplet excited state.



INTRODUCTION

The design and synthesis of photosensitizers capable of harvesting a large fraction of solar light has been the subject of intense investigation due its importance for applications ranging from dye-sensitized solar cells^{1,2} to photocatalytic hydrogen production.^{3–6} In particular, porphyrin derivatives are a class of chromophores possessing favorable photosensitizer properties due to their highly redox-active excited states.^{7,8} However, one drawback of porphyrin derivatives is their relatively poor absorption in the blue-green region of the spectrum (450–550 nm). One strategy of improving the absorption properties of porphyrin derivatives is their functionalization with strongly absorbing boron dipyrin, Bodipy, “antenna” chromophores that are capable of sensitizing the porphyrin-based excited state through efficient intramolecular energy transfer.^{9–19} In the vast majority of Bodipy–porphyrin conjugates, the Bodipy groups are linked to the organic periphery of the porphyrin ring, thus leading to a unidirectional Bodipy to porphyrin energy transfer in a horizontal direction with respect to the porphyrin plane.^{9,11,12,19–22} To the best of our knowledge, there is only a single example where Bodipy moieties are linked to a Sb(V) porphyrin as axial ligands.^{23,24} In addition, Ng and co-workers

studied systems featuring Bodipy chromophores axially bound to Si phthalocyanines^{25,26} or boron subphthalocyanines.²⁷ This synthetic approach offers the benefit of avoiding the elaborate and multistep synthetic procedures usually involved in the preparation of unsymmetrically substituted porphyrins. The organic periphery of the porphyrin is thus left free for further chemical functionalization. In this paper we describe the synthesis and photophysical study of **3** and **6** consisting of a Sn(IV) porphyrin (SnP) with two Bodipy-functionalized phenolate and benzoate axial ligands, respectively. We show that photoexcitation of the Bodipy units at room temperature leads, in the case of **3**, to eventual formation of a charge-separated state, yielding the phenoxyl radical and the porphyrin radical anion, while in the case of **6**, efficient Bodipy to SnP energy transfer leads to the porphyrin-based singlet excited state which converts to the corresponding triplet by intersystem crossing.

Received: December 8, 2011

Published: March 16, 2012

EXPERIMENTAL SECTION

Chemicals. Sn(OH)₂TPP (**2**),²⁸ 4,4-difluoro-8-(4'-hydroxyphenyl)-1,3,5,7-tetramethyl-4-bora-3a,4a-diaza-s-indacene (**1**),²⁹ 4,4-difluoro-8-(4'-carboxyphenyl)-1,3,5,7-tetramethyl-4-bora-3a,4a-diaza-s-indacene (**5**),³⁰ and Sn(OBz)₂TPP (**7**)³¹ were prepared according to published procedures. Chloroform and toluene were kept over activated 3 Å molecular sieves for 24 h prior to use. All other chemicals and solvents were purchased from the usual commercial sources and used as received.

X-ray Crystallography. Suitable crystals of **3** and **4**, grown by slow evaporation of solutions in chloroform/heptane 1:1, and **6**, grown by the slow evaporation of a solution in toluene, were coated in oil and mounted on the goniometer of a STOE IPDS II diffractometer equipped with an image plate detector. Intensity data were collected at 2000 W power (50 kV, 40 mA) with graphite monochromatized Mo K α (λ = 0.71073 Å) radiation. An analytical absorption correction was applied using the program X-RED (routine within the X-AREA software package).

Structures were solved by direct methods using the SIR 92 program³² and refined by full-matrix least-squares on weighted F^2 values for all reflections using the SHELX³³ suite of programs. Non-hydrogen atoms were refined anisotropically. Hydrogen atoms were placed in calculated positions, refined using idealized geometries (riding model), and assigned fixed isotropic displacement parameters. In the crystal structures of **3**, **4**, and **6** the Sn atom lies in a special position and applying the appropriate symmetry elements generates the molecular structures of the corresponding complexes. In the case of compound **6**, a disordered toluene molecule in the asymmetric unit was split and refined isotropically in two positions with approximately 50% site occupancy applying appropriate constraints. Otherwise, refinements of the crystal structures of **3**, **4**, and **6** proceeded smoothly.

Photophysical Measurements. UV–vis absorption spectra were measured on a Shimadzu UV-1700 spectrophotometer using 10 mm path-length cuvettes. Emission spectra were measured on a JASCO FP-6500 fluorescence spectrophotometer equipped with a red-sensitive WRE-343 photomultiplier tube (wavelength range 200–850 nm). Quantum yields were determined from corrected emission spectra following the standard methods³⁴ using rhodamine B (Φ = 0.49 in ethanol),³⁵ 5,10,15,20-tetraphenylporphyrin (Φ = 0.11 in toluene),³⁶ and 5,10,15,20-tetraphenylporphyrinato zinc (Φ = 0.03 in toluene)³⁶ as standards. Emission lifetimes were determined by the time-correlated single-photon counting (TCSPC) technique using an Edinburgh Instruments mini-tau lifetime spectrophotometer equipped with an EPL 405 pulsed diode laser at 406.0 nm with a pulse width of 71.52 ps and a pulse period of 200 ns and a high-speed red-sensitive photomultiplier tube (H5773-04) as detector. Calculations of Förster spectral overlap integrals and critical radii were performed using the PhotochemCAD^{37,38} computer program (version 2.1). Femtosecond transient absorption studies were performed with 420 and 387 nm laser pulses (1 kHz, 150 fs pulse width) from an amplified Ti:Sapphire laser system (Clark-MXR, Inc. CPA 2101), the laser energy was 200 nJ.

Electrochemistry. Cyclic and square wave voltammetry experiments were carried out at room temperature using an AutoLab PGSTAT20 potentiostat and appropriate routines available in the operating software (GPES version 4.9). All measurements were carried out in freshly distilled and deoxygenated dichloromethane with a solute concentration of ca. 1.0 mM in the presence of tetraethylammonium hexafluorophosphate (0.1 M) as supporting electrolyte. A three-electrode cell setup was used with a platinum working electrode, a saturated calomel (SCE) reference electrode, and a platinum wire as counter electrode. All potentials are reported versus the ferrocene/ferrocenium couple (0.43 V versus SCE under the above conditions).

Computational Methods. Density functional theory (DFT) calculations were performed using the GAUSSIAN 03³⁹ suite of quantum chemical programs on triad **3**. The ground state geometries were fully optimized in the gas phase using the atomic coordinates adopted from the X-ray structure. The Becke three-parameter

exchange functional along with the Lee–Yang–Parr correlation functional (B3LYP) has been employed in the study.^{40,41} The LANL2DZ basis set was used for Sn(IV), while the 6-31G(d) basis set was used for all other atoms. No negative frequencies were obtained in the frequency calculation on the optimized structure, indicating the global minima of the geometry in the gas phase. In order to obtain electronic excitations, time-dependent density functional theory (TD-DFT) calculation was carried out on the geometry-optimized structure using the same basis sets. The solvent effect was modeled using the conductor-like polarizable continuum model (CPCM)^{42–44} implemented on the Gaussian 03 package for TD-DFT calculations.

trans-Bis(4,4-difluoro-8-[4-hydroxyphenyl]-1,3,5,7-tetramethyl-4-bora-3a,4a-diaza-s-indaceno)-[5,10,15,20-tetrakis(phenyl)porphyrinato]tin(IV) (3**).** **1** (17 mg, 0.05 mmol) and Sn(OH)₂TPP, **2** (19 mg, 0.025 mmol), were refluxed in dry chloroform (10 mL) under an atmosphere of nitrogen for 12 h. The reaction mixture was left to cool, and the solvent was removed in a rotary evaporator. The solid residue was dissolved in a minimum amount of dichloromethane/hexane 1:1 and passed through a short alumina (activity IV) column. The main band was collected, solvent was removed in a rotary evaporator, and solid was redissolved in chloroform (3 mL). To this solution about 2 mL of heptane was added, and the resulting mixture was left to slowly evaporate, yielding the desired compound in well-formed X-ray-quality crystals (yield 28 mg, 79%).

¹H NMR (300 MHz, CDCl₃): δ (ppm) 0.58 (s, 12H, Bodipy Me); 2.15 (d, J = 9.0 Hz, 4H, Bodipy phenol); 2.39 (s, 12H, Bodipy Me); 5.58 (d, J = 9 Hz, 4H, Bodipy phenol); 5.69 (s, 4H, Bodipy pyrolic); 7.86 (m, 12H, porphyrin meta and para phenylic); 8.24 (m, 8H, porphyrin ortho phenylic); 9.14 (s (Sn satellites J = 15.1 Hz), 8H, porphyrin pyrolic). ¹³C NMR (75 MHz, CDCl₃): δ (ppm) 14.5, 15.2, 118.0, 120.5, 122.0, 123.0, 126.5, 127.3, 128.8, 131.6, 132.9, 134.8, 140.8, 142.9, 147.5, 154.6, 156.8. HRMS (MALDI-TOF): m/z calcd for C₆₃H₄₆BF₂N₆O₂Sn, 1071.2816 [M – Bodipy]⁺; found, 1071.2845.

trans-Bis(phenolato)-[5,10,15,20-tetrakis(phenyl)porphyrinato]tin(IV) (4**).** A modified literature procedure was followed for synthesis of the model compound **4**.⁴⁵ Phenol (4.7 mg, 0.05 mmol) and Sn(OH)₂TPP, **2** (19 mg, 0.025 mmol), were dissolved in toluene (7 mL), and the mixture was stirred at 60 °C for 5 h. The solvent was removed in a rotary evaporator, and the solid was dissolved in chloroform (3 mL). To this solution about 2 mL of heptane was added, and the resulting mixture was left to slowly evaporate, yielding the desired compound in well-formed X-ray-quality crystals (yield 21 mg, 92%).

¹H NMR (300 MHz, CDCl₃): δ (ppm) 1.88 (d, J = 8.1 Hz, 4H, ortho phenol); 5.66 (t, J = 7.2 Hz, 4H, meta phenol); 5.79 (m, 2H, para phenol); 7.81 (m, 12H, porphyrin meta and para phenylic); 8.24 (d, J = 7.2 Hz, 8H, porphyrin ortho phenylic); 9.07 (s, 8H, porphyrin pyrolic). HRMS (MALDI-TOF): m/z calcd for C₅₀H₃₃N₄O₂Sn, 825.1676 [M – phenol]⁺; found, 825.1652.

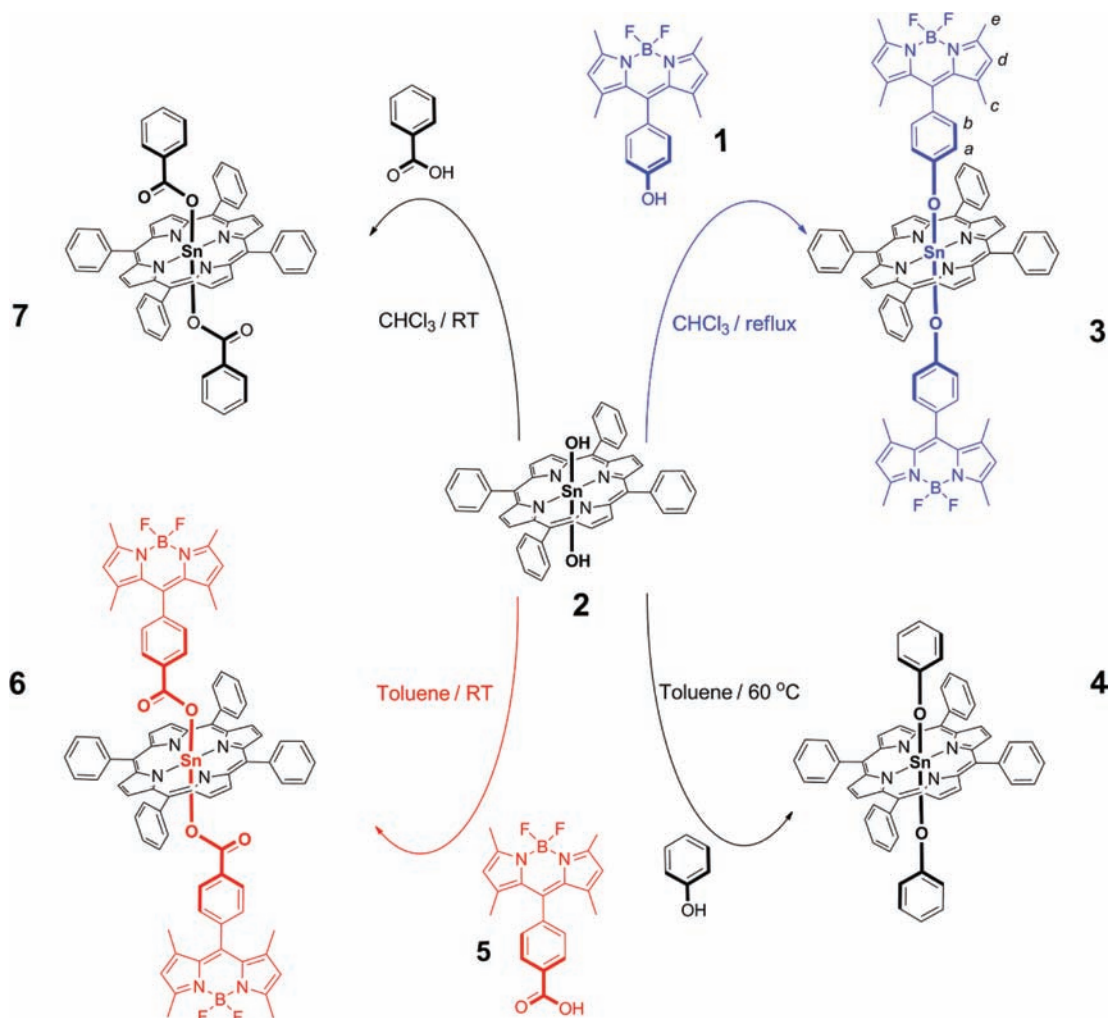
trans-Bis(4,4-difluoro-8-[4-carboxyphenyl]-1,3,5,7-tetramethyl-4-bora-3a,4a-diaza-s-indaceno)-[5,10,15,20-tetrakis(phenyl)porphyrinato]tin(IV) (6**).** **5** (17 mg, 0.05 mmol) and Sn(OH)₂TPP, **2** (19 mg, 0.025 mmol) were stirred at room temperature in dry toluene (10 mL) under an atmosphere of nitrogen for 2 h. The reaction mixture was left to slowly evaporate to yield the desired product as red crystals within 5 days. Product was obtained by filtration and dried under vacuum (yield 27 mg, 74%).

¹H NMR (300 MHz, C₆D₆): δ (ppm) 0.32 (s, 12H, Bodipy methyl); 2.42 (12H, Bodipy methyl); 5.30 (s, 4H, Bodipy pyrolic); 5.39 (d, J = 8.1 Hz, 4H, Bodipy benzylic); 5.54 (d, J = 8.1 Hz, 4H, Bodipy benzylic); 7.45 (m, 12H, porphyrin meta and para phenylic); 8.04 (m, 8H, porphyrin ortho phenylic); 9.10 [s (Sn satellites J = 14.7 Hz), 8H, porphyrin pyrolic]. HRMS (MALDI-TOF): m/z calcd for C₆₄H₄₆BF₂N₆O₂Sn, 1099.2765 [M – Bodipy]⁺; found, 1099.2758.

RESULTS AND DISCUSSION

Synthesis. **3** and **6** and their model compounds **4** and **7** were prepared by reaction of Sn(OH)₂TPP, **2**, with the

Scheme 1. Synthesis of 3 and 6 and Reference Compounds 4 and 7



appropriate phenolate or benzoate ligands as shown in Scheme 1 using modified literature methods.^{31,46–48} **3** was synthesized by reaction of **2** with two equiv of phenol-substituted Bodipy, **1**, in refluxing dry chloroform. Model compound **4** was readily prepared by reaction of **2** with 2 equiv of phenol in toluene at 60 °C. **6** was prepared by addition of 2 equiv of carboxy-substituted Bodipy **5** in a solution of **2** in dry toluene at room temperature. Axial coordination of the Bodipy units to the Sn(IV) porphyrin in **3** and **6** was confirmed by the upfield shift of the signals corresponding to the Bodipy protons in their ¹H NMR spectra (see Figure S1, Supporting Information). The strongest upfield shift is experienced by the signal of the phenolic protons *a* (see Scheme 1) of **3** which shifts from δ 6.7 in **1** to δ 2.2 ppm as a result of their proximity to the porphyrin center, leading to strong shielding by the porphyrin ring current. Less pronounced upfield shifts are observed in the resonances corresponding to the rest of the Bodipy protons of **3**. Also, due to the longer distance between the Bodipy moiety and the porphyrin core, much less pronounced upfield shifts are observed in the carboxylate-bridged **6** (Figure S1, Supporting Information). It is worth mentioning that no splitting or broadening is observed in any of the Bodipy proton signals in both **3** and **6**, indicating that rotation of the Bodipy ligand in solution is fast at the NMR time scale.

Structural Characterization. **3** and **6** along with model compound **4** were characterized by single-crystal X-ray crystallography. The crystal structure of **3** contains two independent molecules in the asymmetric unit. A collection of bond lengths and angles of **3**, **6**, and **4** can be found in Tables S1, S2, and S3, Supporting Information, respectively, while crystallographic details are shown in Table S4, Supporting Information. **3** and **6** consist of two Bodipy–phenolate and Bodipy–benzoate ligands, respectively, axially bound to a distorted octahedral Sn(IV) center of a Sn(IV)TPP moiety (Figure 1 and Figures S2–S5, Supporting Information). In both cases the Bodipy ligands adopt the expected anti conformation about the porphyrin ring, which does not show any distortion from planarity.⁴⁷ In **3**, the average Sn–O–C angle, 125°, and average Sn–O distance, 2.062 Å, are in good agreement with those found in other Sn(IV) porphyrin phenolates.^{47,49–51} Similarly, the average Sn–O distance in **6**, 2.095 Å, is well within the expected range for a Sn(IV) porphyrin carboxylate complex.^{31,46} The angles between the mean planes of the Bodipy units and those of the phenolate groups in **3** average at 77°. This deviation from the expected orthogonality is attributed to the steric hindrance induced by the porphyrin ring. In contrast, in **6** the benzoate ring is almost perpendicular to the mean plane of the Bodipy unit (83°) due to the greater average distance between the porphyrin and the Bodipy groups.

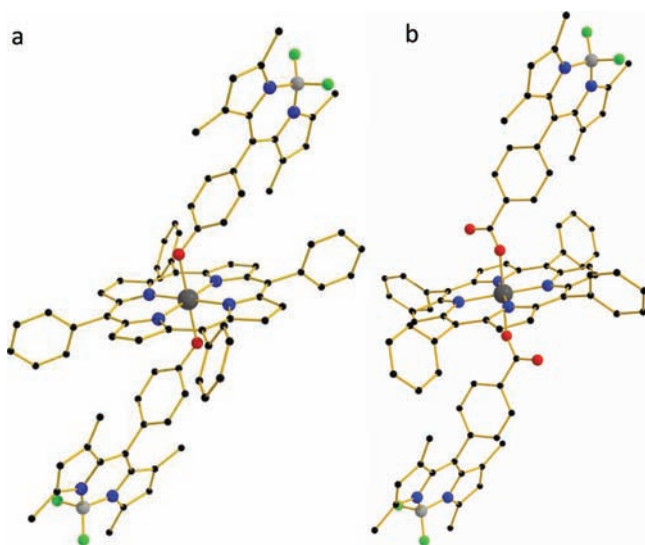


Figure 1. Molecular structures of (a) one of the two independent molecules of **3** found in the unit cell of $3 \cdot 2\text{CHCl}_3$ and (b) **6** taken from the crystal structure of $6 \cdot 2\text{C}_7\text{H}_8$. Solvent molecules and hydrogen atoms are omitted for clarity. Color code: carbon, black; nitrogen, blue; oxygen, red; boron, light gray; fluorine, green; tin, dark gray.

In both **3** and **6**, the Bodipy moieties are unremarkable, showing the usual tetrahedral arrangement about the boron atom with B–F and B–N distances averaging at 1.393 and 1.552 Å, respectively.

The structure of **4** (Figure S6 and Table S3, Supporting Information) is unremarkable and correlates well with the structures of other Sn(IV) porphyrin phenolates.^{47,49–51}

Electrochemical Study. The redox behavior of **3** and **6** and their reference compounds **1**, **2**, **4**, and **7** was studied by cyclic and square wave voltammetry in dichloromethane using ferrocene as an internal standard. The redox data are summarized in Table 1, and representative cyclic voltammograms are shown in Figure 2. The first reversible oxidation wave shown by **3** and **6** between 0.72 and 0.76 V vs Fc/Fc⁺ is attributed to simultaneous oxidation of the two Bodipy units to the corresponding cationic radicals.^{52–54} Additionally, **3** shows a second irreversible oxidation wave, which is assigned to oxidation of the coordinated phenolic groups of the SnP moiety to the corresponding phenoxyl radicals.^{48,55,56} **3** also shows two reversible reduction waves: the first (–1.41 V vs Fc/Fc⁺) corresponds to porphyrin-based reduction and the second (–1.81 V vs Fc/Fc⁺) to simultaneous reduction of the coordinated Bodipy units. It is noteworthy that the Bodipy-based reduction of **3** is considerably shifted to more negative potentials (by 0.09 V) compared to that of reference compound **1**. This is attributed to the electrostatic effects induced by the

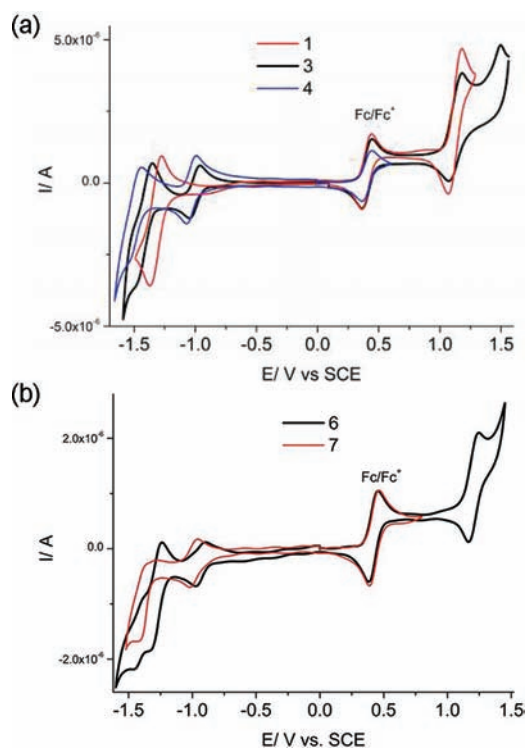


Figure 2. (a) Cyclic voltammograms of triads **3** and **6** and reference compounds **1**, **4**, and **7** in dry dichloromethane using a saturated calomel electrode (SCE) as reference at a scan rate of 100 mVs^{-1} . (b) Fc/Fc⁺ denotes the redox couple of ferrocene, which was used as an internal standard.

reduced porphyrin. The anticipated second porphyrin-based reduction of **3** occurs outside of the solvent window as is rendered more difficult due to the electrostatic repulsion induced by the reduced Bodipy groups. **6** shows three consecutive reversible reduction waves (–1.38, –1.73, and –1.87 V vs Fc/Fc⁺) attributable to the first porphyrin, Bodipy, and second porphyrin-based reductions respectively. These assignments are further supported by the results of the DFT calculation on **3** and **6** vide infra, which show that the highest occupied molecular orbitals (HOMOs) possess predominantly Bodipy character, while the lowest unoccupied molecular orbitals (LUMOs) are located on the porphyrins.

Photophysical Properties. Electronic Spectra. UV–vis absorption spectra of compounds **1–4** and **6** and **7** are shown in Figure 3. **3** and **6** show a combination of absorption features from their two constituent chromophores. The intense peak at ca. 500 nm corresponds to the lowest energy π – π^* transitions of the Bodipy chromophores,^{52–54} while the strong absorption at 425 nm and the two weaker transitions at ca. 560 and 600

Table 1. Redox Data of Compounds **1–4**^a

compound	$E_{1/2}^{\text{Red}^1}/\text{V}$ ($\Delta E_p/\text{V}$) ^b	$E_{1/2}^{\text{Red}^2}/\text{V}$ ($\Delta E_p/\text{V}$) ^b	$E_{1/2}^{\text{Red}^3}/\text{V}$	$E_{1/2}^{\text{Ox}^1}/\text{V}$ ($\Delta E_p/\text{V}$)	$E_{1/2}^{\text{Ox}^2}/\text{V}$ ($\Delta E_p/\text{V}$)
1	–1.72 (0.09)			0.73 (0.08)	
2	–1.42 (0.09)	–1.82 (0.12)		1.04 (irrev.)	
3	–1.41 (0.08)	–1.81 (0.12)		0.72 (0.10)	1.08 (irrev.)
4	–1.43 (0.08)	–1.89 (0.10)		0.65 (irrev.)	
6	–1.38 (0.08)	–1.73 (0.09)	–1.87 (0.07)	0.76 (0.08)	
7	–1.42 (0.05)	–1.83 (irrev.)			

^aAll potentials are reported vs the ferrocene/ferrocenium (Fc/Fc⁺) redox couple. Unless otherwise noted, all waves are reversible. ΔE_p of the Fc/Fc⁺ redox couple is 0.07 V. The error on the reported potentials is 0.1 mV. ^bThe anodic – cathodic peak separations are given in parentheses.

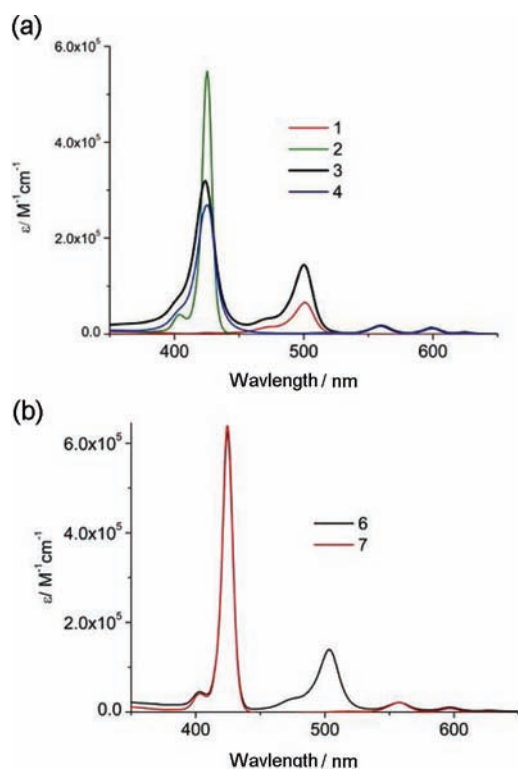


Figure 3. UV-vis absorption spectra of compounds (a) 1–4 and (b) 6 and 7 in toluene.

nm are due to the SnP-based Soret and Q bands, respectively.⁴⁶ These attributions are consistent with the results of time-dependent DFT calculations on **3** *vide infra*. It is worth mentioning that the absorption features of **3** are slightly blue shifted by 1–3 nm compared to the corresponding transitions of the model compounds **1** and **2**. In addition, the Soret band of **3** is broader and has lower oscillator strength compared to that of **2** (Figure 3). These effects have been observed in model compound **4** and in other Sn(IV) porphyrin complexes with phenolate axial ligands.^{45,46,56,57} As seen in Figure 3, the absorption spectra of **3** and **6** are largely superpositions of those of **1** and **4** and **1** and **7**, respectively, indicating weak interactions between the porphyrin and Bodipy chromophores in the ground state.

Emission Spectra at Room Temperature. The emission spectra of **1**–**4** in toluene solutions at room temperature are

shown in Figure 4, while selected emission data are listed in Table 2. **1** shows the typical bright fluorescence of Bodipy at

Table 2. Emission Data for Compounds 1–7 in Toluene at Room Temperature

compound	$\lambda_{\text{max}}/\text{nm}$ ($\lambda_{\text{exc}}/\text{nm}$)	Φ	τ (ns)
1	513 (488)	0.64	3.7
2	607, 660 (560)	0.035	1.6
3	513 (478)	~0.003	<1
4	606, 659 (560)	~0.003	<1
5	516 (488)	0.57	2.6
6	605, 657 (557)	0.020	<1 ^a 1.3 ^b
7	604, 656 (557)	0.021	1.3

^aUsing a ± 40 nm interference filter centered at 500 nm to monitor Bodipy residual fluorescence. ^bUsing a ± 40 nm interference filter centered at 670 nm to monitor Sn porphyrin fluorescence.

513 nm when excited at 488 nm. In **3** the Bodipy emission is strongly quenched as shown in Figure 4a, where the fluorescence spectra of isoabsorbing solutions of **1** and **3** are compared. The observed quenching of the Bodipy-based emission can be explained on the basis of photoinduced energy transfer from the Bodipy $^1\pi-\pi^*$ excited state to the lower lying singlet excited state of the porphyrin and/or to the existence of new nonradiative pathways from the Bodipy $^1\pi-\pi^*$ state to the ground state. In addition, no SnP-based emission could be detected at room temperature when **3** was selectively excited at the Bodipy chromophore (488 nm, Figure 4a), and only a very weak emission was detected upon excitation of the SnP unit (560 nm, Figure 4b). **4** also shows strongly quenched fluorescence compared to its hydroxyl counterpart **2**, in agreement with what is observed in similar phenolate Sn(IV) porphyrin complexes.^{23,58,59} This quenching has been attributed to electron transfer from the phenolate ligand to the excited porphyrin.⁵⁹ In fact, excitation of Bodipy in **3** into its first $^1\pi-\pi^*$ excited state, as shown by transient absorption experiments *vide infra*, leads to rapid energy transfer to the corresponding porphyrin-based singlet excited state, which is, in turn, reductively quenched by the phenolate moiety.

The emission spectra of **6** and **7** in toluene solution at room temperature are shown in Figure 5, while selected emission data are given in Table 2. In contrast to **3**, selective excitation of Bodipy of **6** shows a strongly quenched Bodipy-based emission accompanied by fluorescence from the porphyrin with maxima

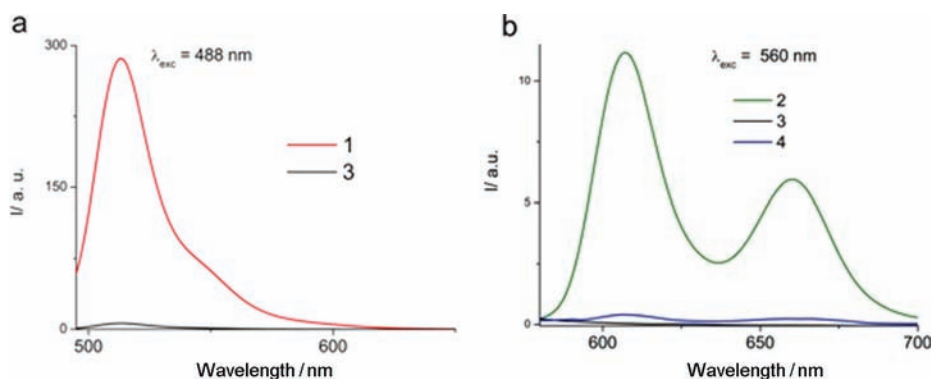


Figure 4. Room-temperature fluorescence spectra of isoabsorbing ($A = 0.1$) toluene solutions of (a) **1** and **3** exciting at 488 nm (Bodipy chromophore) and (b) **2**, **3**, and **4** exciting at 560 nm (SnTPP chromophore).

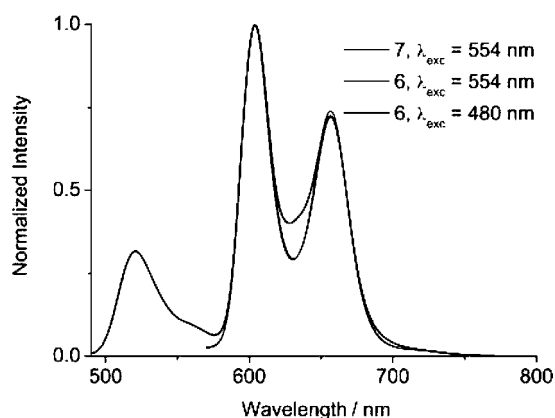


Figure 5. Normalized room-temperature emission spectra of **6** and **7** in toluene exciting at either 480 (Bodipy chromophore) or 554 nm (SnP chromophore).

at 604 and 656 nm (Figure 5). The excitation spectrum of **6** monitoring at 657 nm, shown in Figure 6, reveals a pronounced

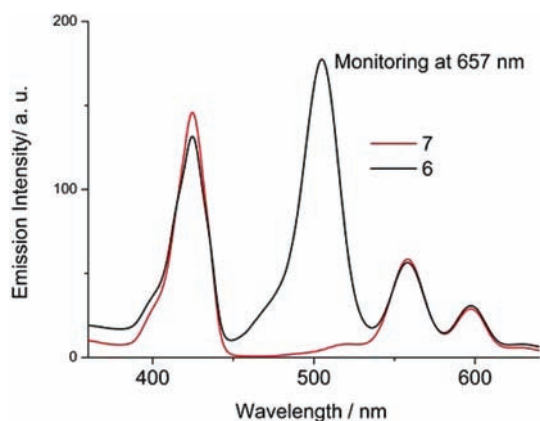


Figure 6. Uncorrected excitation spectra of **6** and **7** in toluene monitoring at the porphyrin-based fluorescence.

Bodipy absorption feature at ca. 500 nm. This is a clear indication of photoinduced energy transfer from the $^1\pi-\pi^*$ excited state of the Bodipy chromophore to the lower lying singlet excited state of the porphyrin unit, leading to sensitized fluorescence from the latter. In **6**, we observe no quenching of the porphyrin-based emission as, contrary to **3**, electron transfer between the benzoate functionality and the Sn(IV) porphyrin chromophore does not occur.

Emission Spectra at 77 K. To shed more light on the processes taking place upon photoexcitation of **3** and **6**, a series of experiments was performed in toluene glass at 77 K. The emission spectra of **3** and **4** at 77 K after excitation at 560 nm are shown in Figure 7. The most striking difference in comparison to the room-temperature spectra of Figure 4 is the restoration of porphyrin-based fluorescence ($\lambda_{\max} \approx 600$ and 660 nm) in phenolate complexes **3** and **4**. This observation is in agreement with the results obtained in the study of other two-component systems, in which photoinduced electron transfer, readily occurring at room temperature, is suppressed in frozen solvents at 77 K.^{60–62} This is a result of destabilization of charge-separated states due to lack of solvent reorganization. One more interesting feature seen in the low-temperature emission spectra of **3** and **4** is a relatively weak emission at ca.

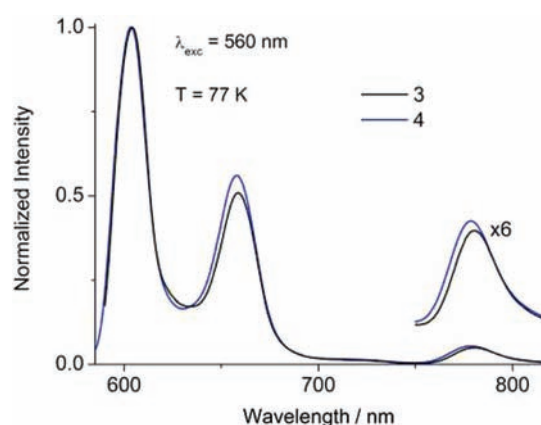


Figure 7. Normalized emission spectra of **3** and **4** in toluene glass at 77 K after selective excitation of the Sn(IV) porphyrin chromophore at 560 nm.

780 nm that is due to phosphorescence. The long lifetime of this low-energy emission (ca. 20 ms) confirms its spin-forbidden nature. The excitation spectrum of **3** at 77 K (Figure 8) monitoring at both the fluorescence (660 nm) and the

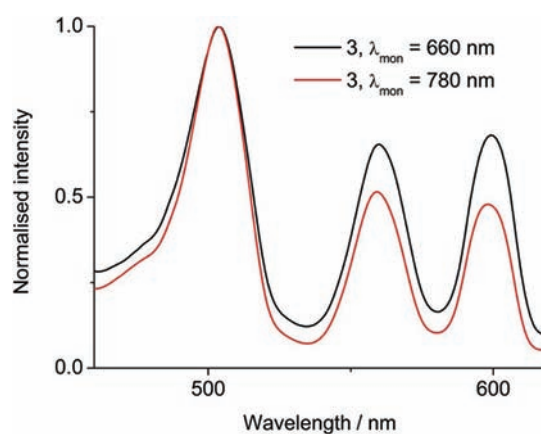


Figure 8. Normalized excitation spectra of **3** in toluene glass at 77 K monitoring at 660 and 780 nm.

phosphorescence (780 nm) emissions reveals absorption features of both the SnP and the Bodipy chromophores. This is unambiguous evidence that selective excitation of the Bodipy chromophores of **3** into their $^1\pi-\pi^*$ excited state is followed by energy transfer to the first singlet excited state of the porphyrin unit, which then partly undergoes intersystem crossing to the corresponding triplet.

6 exhibits almost identical behavior with **3**, as can be seen in the emission spectra of **6** and **7** at 77 K after selective excitation at both the Bodipy and the porphyrin chromophores which are shown in Figure 9. Studies on the Bodipy chromophore in combination with $[\text{Ru}(\text{bipy})_3]^{2+}$ -type units (bipy = 2,2'-bipyridine) have revealed a Bodipy-based phosphorescence emission at ca. 770–790 nm with a lifetime in the range of tens of milliseconds.⁵⁴ The fact that in **3** and **6** the Bodipy $^3\pi-\pi^*$ excited state lies at similar energy to the $^3\text{SnP}^*$ state suggests that a thermal equilibrium between the two states is possible in **3** and **6**. Such bidirectional triplet energy transfer leading to a long-lived triplet equilibrated excited state has been shown to occur in an array combining the Bodipy chromophore with a Pt(II) tetrabenzoporphyrin.¹² Thus, as the Jablonski diagram in

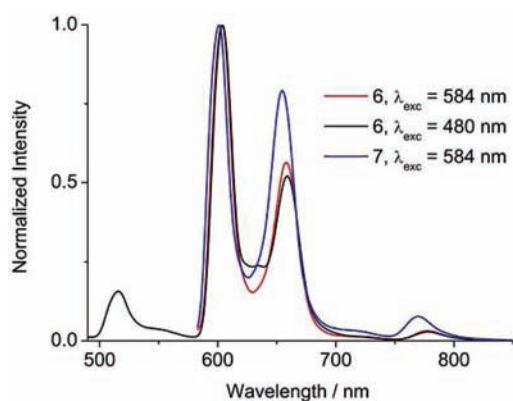


Figure 9. Emission spectra of **6** and **7** in frozen toluene glass at 77 K.

Figure 10 shows, excitation of **3** into the Bodipy-based $^1\pi-\pi^*$ excited state is followed by energy transfer to the porphyrin-

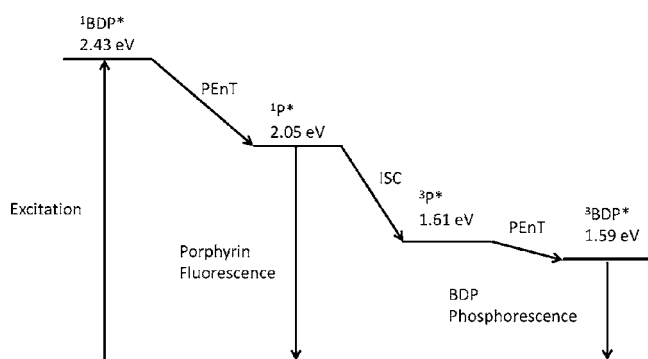


Figure 10. Jablonski diagram of the processes that take place after selective excitation of the Bodipy chromophore of **3** and **6** at 77 K. Energies given are those calculated for **3**; however, the ones for **6** are almost equal (see Figure 13). $^1\text{BDP}^*$ and $^1\text{P}^*$ denote the Bodipy and porphyrin-based singlet excited states, respectively, while $^3\text{BDP}^*$ and $^3\text{P}^*$ denote the corresponding triplets. PEnt stands for photoinduced energy transfer and ISC for intersystem crossing.

based $^1\text{SnP}^*$ excited state, which, in turn, partly decays radiatively (fluorescence) to the ground state and partly intersystem crosses to the $^3\text{SnP}^*$ excited state, which gives rise to phosphorescence.⁶³

Transient Absorption Spectroscopy. Femtosecond transient absorption spectroscopy provided further insight into the excited state reactions in **3** and **6**, especially to corroborate the energy transfer. To this end, **3** and **6** and model compounds **1**, **4**, and **7** were probed with 150 fs laser pulses at either 420 or 490 nm to excite the porphyrin or Bodipy. For the model complexes **4** and **7**, the porphyrin singlet excited state characteristics, which evolve with a lifetime of 0.4 ± 0.1 ps from higher lying excited states that are formed upon 420 nm excitation, include minima at 435, 560, 600, and 660 nm and a broad maximum of absorption between 445 and 600 nm, see Figure S7, Supporting Information. It is interesting to note that the bleaching at 435, 560, and 600 nm correlates nicely with the transition seen in the ground state spectrum of **4** and **7** (Figure 3). In **7** (Figure S7, Supporting Information), the singlet excited state is subject to intersystem crossing and forms within 1400 ± 100 ps of the corresponding triplet excited state. The most significant spectral features of the latter are maxima at 480 and 815 nm as well as minima at 560 and 600 nm. In stark

contrast, the singlet excited state in **4** (Figure S8, Supporting Information) decays rather rapidly and undergoes electron transfer with a lifetime of 4 ± 2 ps vide supra. The main spectral features of this product are maxima at 515, 585, 620, 645, 710, 760, and 825 nm, which resemble the spectral features of the one-electron-reduced porphyrin.^{64–66} The product of the one-electron oxidation of the phenolate ligand is, however, masked by the porphyrin-centered features. In fact, it is known to absorb below 400 nm.^{67,68} This initial electron transfer is accompanied by a second, slower decay with a lifetime of 20 ± 5 ps to yield a transient with maxima at 460, 485, 545, 585, 615, and 645 nm and is probably due to structural rearrangement. In addition, a long-lived component of 450 ± 50 ps is noted, which reinstates the singlet ground state and, as such, reflects the charge recombination.

Next, **1** (see Figure S9, Supporting Information) was excited at 490 nm. The transient absorption changes, as they are formed immediately after the laser pulse, are dominated by ground state bleaching in the 510 and 560 nm range, a finding that is well in line with previous investigations,^{11,19,53,54,69} and a maximum at 435 nm. These features decay within 3.5 ± 0.5 ns in toluene to the corresponding triplet excited state.

Different is the picture when using 420 or 490 nm to excite Bodipy and SnP or Bodipy, respectively, in the Bodipy–porphyrin conjugates **3** and **6**. Initially after the laser pulse, formation of the singlet excited state of Bodipy is detected with transient minima at in the 510 and 560 nm range, see Figures 11 and 12. In contrast to **1**, the decay of the singlet excited state is remarkably fast and completed within 3.5 ± 1 ps in the case of **6** (Figure 11). The product of this decay process is not the triplet excited state of Bodipy but rather the porphyrin singlet excited state, as determined from the observation of the characteristic spectral features throughout the visible and near-infrared part of the spectrum (i.e., minima at 435, 560, 600, and 660 nm as well as a broad maximum between 445 and 600 nm). Importantly, the porphyrin singlet excited state formation kinetics are a qualitative match for those corresponding to the Bodipy singlet excited state decay. The correspondingly formed porphyrin singlet excited state intersystem crosses, as in **7**, to the triplet manifold. Likewise, photoexcitation of **3** at 490 nm is best described as a process that forms the Bodipy singlet excited state (Figure 12). The closer proximity between Bodipy and porphyrin in **3** induces a faster energy transfer decay of 2.0 ± 0.5 ps than that seen in the carboxy-bridged **6**. The main product of the decay is, as in **6**, the singlet excited state of the porphyrin. In the latter, a charge transfer state evolves, however, as verified by the characteristic features at 460, 485, 545, 585, 615, and 645 nm and by the characteristic charge transfer dynamics of 4 ± 2 ps vide supra. From here a biexponential decay with lifetimes of 20 ± 5 and 450 ± 50 ps is seen, which are associated with structural rearrangement of the charge transfer state and charge recombination, respectively, vide supra. At this point we attempt to comment on the mechanism of Bodipy to porphyrin energy transfer in **3** and **6**. Assuming a Förster-type resonance energy transfer, FRET, mechanism⁷⁰ we calculate a predicted FRET rate, k_{FRET} , using eqs 1 and 2

$$k_{\text{FRET}} = \frac{1}{\tau_{\text{D}}} \left(\frac{R_{\text{c}}}{r_{\text{DA}}} \right)^6 \quad (1)$$

$$R_{\text{c}}^6 = \Phi_{\text{D}} \kappa^2 J(\lambda) \quad (2)$$

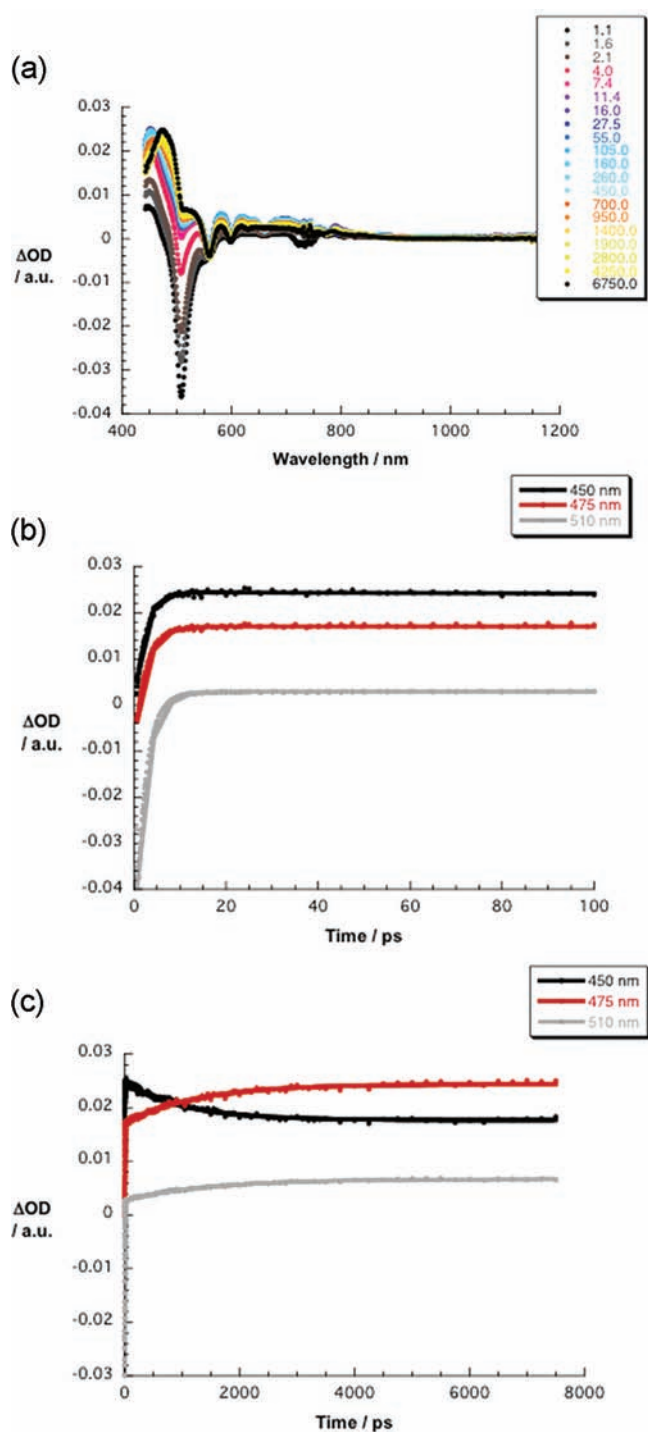


Figure 11. (a) Differential absorption spectra (visible and near-infrared) obtained upon femtosecond flash photolysis (490 nm, 120 nj) of **6** in toluene with several time delays between 1.1 and 6750 ps at room temperature; see figure legend for details about time evolution. (b) Time-absorption profiles of spectra at 450, 475, and 510 nm monitoring the energy transfer (i.e., 3.5 ± 1 ps). (c) Time-absorption profiles of spectra at 450, 475, and 510 nm monitoring the intersystem crossing (i.e., 1400 ± 100 ps).

where τ_D is the fluorescence lifetime of the donor, R_c is the Förster critical radius, r_{DA} is the donor-acceptor distance, Φ_D is the fluorescence quantum yield of the donor, $J(\lambda)$ is the Förster overlap integral between the emission spectrum of the donor and the absorption spectrum of the acceptor, and κ^2 is a factor

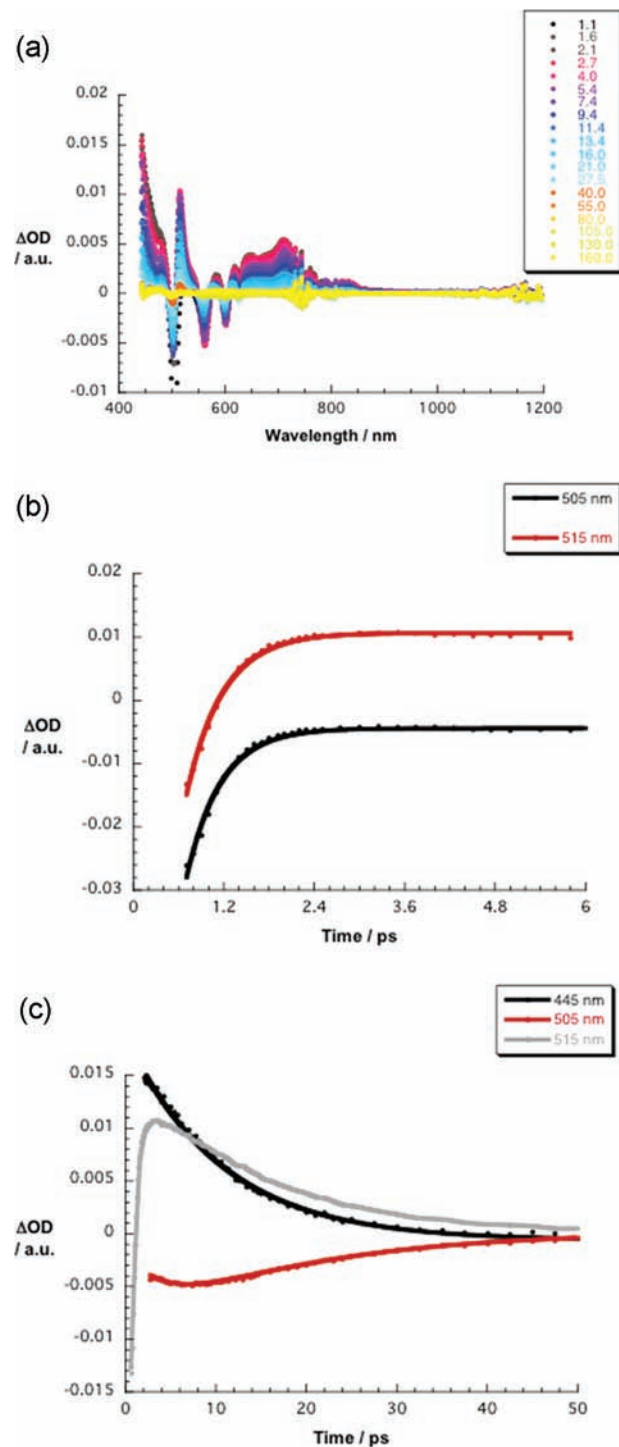


Figure 12. (a) Differential absorption spectra (visible and near-infrared) obtained upon femtosecond flash photolysis (490 nm, 120 nj) of **3** in toluene with several time delays between 1.1 and 160 ps at room temperature; see figure legend for details about time evolution. (b) Time-absorption profiles of spectra at 505 and 515 nm monitoring energy transfer (i.e., 2.0 ± 0.5 ps). (c) Time-absorption profiles of spectra at 445, 505, and 515 nm monitoring the charge transfer (i.e., 4 ± 2 ps) and structural rearrangement of the charge transfer state (i.e., 20 ± 5 ps).

related to the relative orientation of the donor and acceptor transition dipoles.^{71,72} For **3** and **6** using the spectroscopic data in Table 2, taking r_{DA} as the B-Sn distance in the crystal structures of **3** (10.1 Å) and **6** (11.2 Å) and taking $\kappa^2 = 2/3$

(dynamically averaged orientation^{70,71}) gives critical radii of 36.3 and 36.6 Å and energy transfer rate constants of 5.9×10^{11} and $4.7 \times 10^{11} \text{ s}^{-1}$, respectively. The experimentally determined rate constants ($1/\tau$) are 5.0×10^{11} and $2.9 \times 10^{11} \text{ s}^{-1}$ for **3** and **6**, respectively, and agree remarkably well with the computed ones in both trend and magnitude. Additionally, the results of DFT calculations on geometry-optimized models of **3** and **6**, *vide infra*, show no significant orbital overlap between the Bodipy and the porphyrin, thus precluding the existence of Dexter exchange energy transfer⁷³ pathways. It should, however, be noted that in solution there may be some transient geometrical orientations, in which the orbital overlap between the Bodipy and the porphyrin is significant. In light of the aforementioned, we cannot completely rule out a contribution from the Dexter mechanism.⁷⁴ However, given the good agreement between experimental and theoretical values (assuming exclusively FRET mechanism) and taking into account the results of DFT calculations on **3** and **6** we conclude that Bodipy to porphyrin energy transfer takes place predominantly by the Förster mechanism.

In summary, selective excitation of Bodipy units in **3** and **6** leads, in both cases, to the population of the porphyrin-based singlet excited state by rapid Bodipy to porphyrin energy transfer. However, as shown in the Jablonski diagrams of Figure 13, the fates of the porphyrin singlet excited states in **3** and **6** are quite different. In the case of **3**, as a result of the tendency

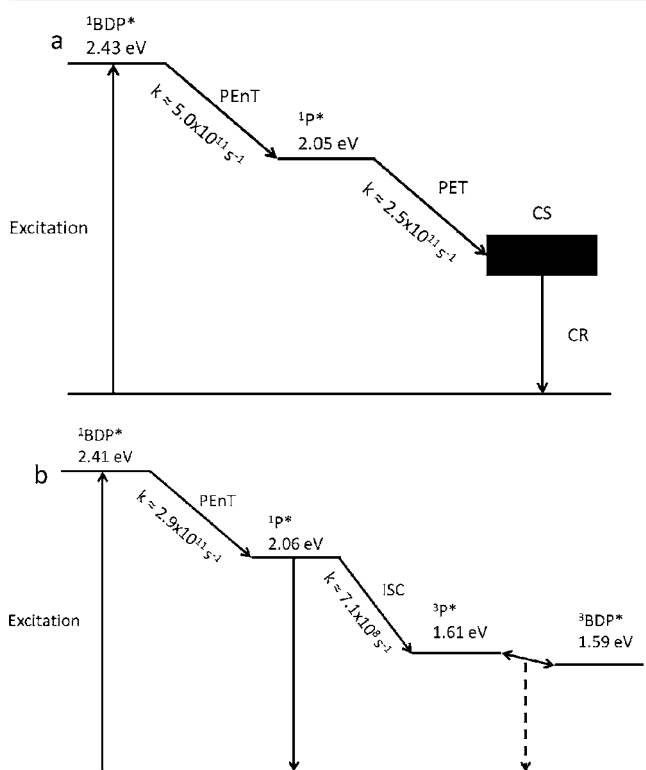


Figure 13. Jablonski diagrams illustrating the processes that take place after photoexcitation of the Bodipy part of (a) **3** and (b) **6** at room temperature. Rate constants, k , of the processes as measured by transient absorption spectroscopy are also shown. $^1\text{BDP}^*$ and $^1\text{P}^*$ denote the Bodipy and porphyrin-based singlet excited states, respectively, while $^3\text{BDP}^*$ and $^3\text{P}^*$ denote the corresponding triplets. PET stands for photoinduced electron transfer, PEnt for photoinduced energy transfer, and ISC for intersystem crossing. Dashed arrow denotes radiationless decay.

of phenolate ligands to oxidize to the corresponding phenoxyl radicals,^{59,75,76} the porphyrin singlet excited state converts to a charge-separated state due to phenolate to porphyrin electron transfer. The existence of this electron transfer pathway in **3** is responsible for rapid deactivation of the porphyrin singlet excited state, leading to the observed almost complete absence of porphyrin-based fluorescence at room temperature (Figure 4). In contrast, the presence of the nonoxidizable benzoate linker in **6** results in formation of a stable porphyrin-based singlet excited state following Bodipy to porphyrin energy transfer. This singlet excited state, as expected, partly converts to the ground state by fluorescence and partly undergoes intersystem crossing to form the corresponding porphyrin triplet excited state.

DFT Calculations. Theoretical DFT calculations were performed on **3** and **6** at the B3LYP level of theory using the 631-G* basis set. The frontier orbitals of **3** and **6** were generated from the gas-phase-optimized geometries (a list of Cartesian coordinates can be seen in Tables S5 and S6, Supporting Information) and are shown in Figures 14 and 15,

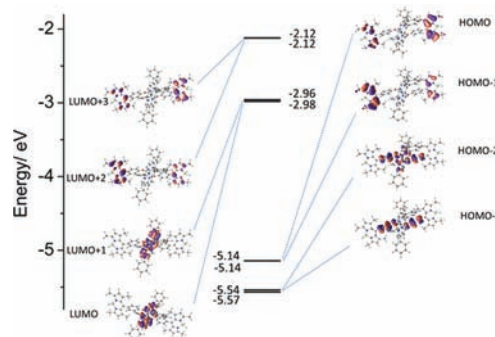


Figure 14. Frontier orbitals obtained from gas-phase DFT calculation on conjugate **3** (see main text for details).

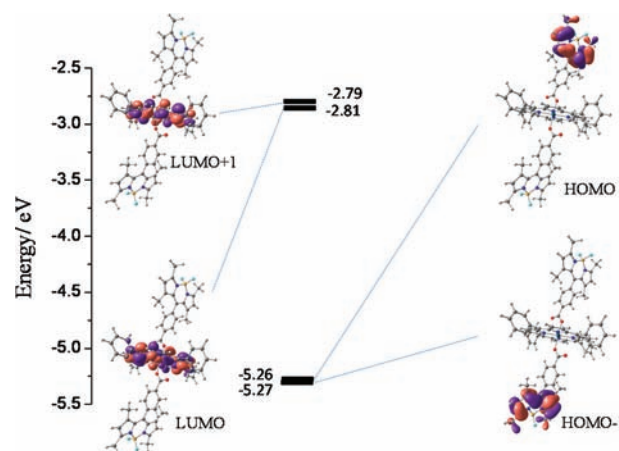


Figure 15. Frontier orbitals obtained from gas-phase DFT calculation on conjugate **6** (see main text for details).

respectively. The HOMO and HOMO–1 orbitals of **3** (Figure 14) are almost degenerate in energy and π -bonding orbitals located on the Bodipy moieties. The LUMO and LUMO+1 lie closely in energy and are π -antibonding orbitals of porphyrin character. The TD-DFT calculation predicts three intense closely spaced singlet electronic transitions at 398, 399, and 400 nm with oscillator strengths of 1.72, 0.98, and 0.31, respectively (Table S7, Supporting Information). The first two are of

HOMO–5 to LUMO+1 and HOMO–5 to LUMO character, respectively (porphyrin-based π – π^* transitions), and correspond to the experimentally observed Soret band. The third transition at 400 nm (mainly HOMO–4 to LUMO+3) corresponds to a phenolate to Bodipy charge transfer transition. In addition, a clearly Bodipy-based π – π^* (predominantly HOMO–1 to LUMO+3 and HOMO to LUMO+2) transition at 423 nm is predicted and corresponds to the experimentally observed band at 500 nm. As can be seen in Figure S10, Supporting Information, which compares the experimental absorption spectrum of **3** with the calculated one, the energy of the predicted Bodipy-based transition is much higher compared to that of the observed absorption band. However, TD-DFT calculations are known for overestimating the energy of the lowest singlet transition in Bodipy chromophores.^{69,77} Finally, the two lowest energy bands predicted at 577 and 582 nm with oscillator strengths of 0.03 and 0.04, respectively, are of mixed porphyrin π – π^* and phenolate to porphyrin charge transfer character (predominantly HOMO–2 to LUMO+1 and HOMO–2 to LUMO, respectively). The partial phenolate to porphyrin charge transfer nature of the lowest energy transitions in **3** is in agreement with the experimentally observed formation of a charge-separated state resulting from phenolate to porphyrin electron transfer following selective excitation of the Bodipy chromophore.

In the case of **6**, the HOMO and HOMO–1 orbitals are almost degenerate in energy and possess Bodipy π character, while the LUMO and LUMO+1 are π -antibonding orbitals of porphyrin character (Figure 15). The TD-DFT calculation predicts two closely spaced intense transitions at 399 and 401 nm (oscillator strengths of 1.25 and 0.96, respectively) and one at 422 nm (oscillator strength 0.78). The first two are mainly of HOMO–3 to LUMO+1 and HOMO–3 to LUMO character, respectively (porphyrin-based π – π^* transitions corresponding to the Soret band), while the third transition possesses mainly HOMO to LUMO+3 character (Bodipy-based π – π^* transitions). As in **3**, the TD-DFT calculation considerably overestimates the energy of the Bodipy-based π – π^* transition (Figure S11, Supporting Information).^{69,77} Lower intensity transitions of HOMO–2 to LUMO+1 and LUMO character (porphyrin-based π – π^* transitions corresponding to the Q bands) are predicted at 550 and 552 nm (oscillator strengths 0.02 and 0.03, respectively). It is worth noting that the low-energy transitions predicted for **6**, contrary to those of **3** (see discussion above), do *not* possess any benzoate to porphyrin charge transfer character (Table S7, Supporting Information). This is in agreement with the observed lack of electron transfer in the room-temperature emission and transient absorption spectrum of conjugate **6**.

CONCLUSIONS

3 and **6**, consisting of two Bodipy-functionalized phenolate and benzoate ligands, respectively, axially bound to a Sn(IV) porphyrin, were synthesized and structurally characterized. The absorption spectra and electrochemical studies on **3** and **6** show that the Bodipy and porphyrin chromophores interact only weakly in the ground state. However, the almost complete absence of photoemission from **3** at room temperature suggests that, in the excited state, energy and/or electron transfer might be taking place. Indeed, as transient absorption experiments show, selective excitation of the Bodipy unit in **3** results in rapid ($k = 5.0 \times 10^{11} \text{ s}^{-1}$) decay of the Bodipy-based singlet excited state and concomitant formation of the Sn(IV) porphyrin-

based singlet excited state which is quenched by formation of a charge-separated state resulting from phenolate to porphyrin electron transfer. Contrary to **3**, the carboxy-bridged Bodipy–porphyrin conjugate **6** shows strongly quenched Bodipy fluorescence and sensitized porphyrin emission upon selective excitation of the Bodipy unit. Transient absorption measurements on **6** show rapid Bodipy to Sn(IV) porphyrin singlet energy transfer ($k = 2.9 \times 10^{11} \text{ s}^{-1}$) leading to a stable porphyrin singlet excited state, which deactivates by fluorescence and intersystem crossing to the corresponding triplet state ($\tau = 1.4 \text{ ns}$). Emission experiments at 77 K in frozen toluene show that the electron transfer pathway observed in **3** at room temperature is suppressed. Instead, in both **3** and **6**, excitation of the Bodipy unit results in population of the first singlet excited state of the Sn(IV) porphyrin chromophore. Subsequently, intersystem crossing leads to phosphorescence from the Bodipy triplet excited state. The above results suggest that improvement of the light harvesting ability of a Sn(IV) porphyrin is better achieved by use of a benzoate bridge to link to a Bodipy sensitizer compared to use of a phenolate linker. This is because the benzoate bridge effectively mediates sensitization of the Sn(IV) porphyrin excited state without providing electron transfer pathways, which rapidly quench it as occurs in the case of a phenolate bridge. The Sn(IV) porphyrin excited state may then be used as an electron donor/acceptor in a photocatalytic or photocurrent scheme.

ASSOCIATED CONTENT

Supporting Information

X-ray crystallographic data for 3·2CHCl₃, 6·2C₇H₈, and 4·2CHCl₃ in CIF format; ¹H NMR spectra of **1**, **3**, and **6**; ORTEP views, selected bond lengths and angles, and crystallographic data of 3·2CHCl₃, 6·2C₇H₈, and 4·2CHCl₃; transient absorption spectra of **7**, **4**, and **1**; experimental and calculated absorption spectra of **3** and **6**; Cartesian coordinates of the optimized geometries of **3** and **6**; TDDFT-calculated singlet electronic transitions of **3** and **6**. This material is available free of charge via the Internet at <http://pubs.acs.org>.

AUTHOR INFORMATION

Corresponding Author

*E-mail: coutsole@chemistry.uoc.gr (A.G.C.); dirk.guldi@chemie.uni-erlangen.de (D.M.G.).

Notes

The authors declare no competing financial interest.

ACKNOWLEDGMENTS

The European Commission funded this research by FP7-REGPOT-2008-1, Project BIOSOLENUTI No 229927, Heraklitos grant from Ministry of Education, and GSRT. In addition, financial support from the DFG (Cluster of Excellence and SFB 583) and the BMBF is greatly acknowledged.

REFERENCES

- (1) Hagfeldt, A.; Boschloo, G.; Sun, L. C.; Kloo, L.; Pettersson, H. *Chem. Rev.* **2010**, *110*, 6595–6663.
- (2) Yum, J. H.; Baranoff, E.; Wenger, S.; Nazeeruddin, M. K.; Gratzel, M. *Energy Environ. Sci.* **2011**, *4*, 842–857.
- (3) Wang, X. H.; Goeb, S.; Ji, Z. Q.; Pogulaichenko, N. A.; Castellano, F. N. *Inorg. Chem.* **2011**, *50*, 705–707.

- (4) Kluwer, A. M.; Kapre, R.; Hartl, F.; Lutz, M.; Spek, A. L.; Brouwer, A. M.; van Leeuwen, P. W. N. M.; Reek, J. N. H. *Proc. Natl. Acad. Sci. U.S.A.* **2009**, *106*, 10460–10465.
- (5) Yamaguchi, H.; Onji, T.; Ohara, H.; Ikeda, N.; Harada, A. *Bull. Chem. Soc. Jpn.* **2009**, *82*, 1341–1346.
- (6) Kim, W.; Tachikawa, T.; Majima, T.; Li, C.; Kim, H. J.; Choi, W. *Energy Environ. Sci.* **2010**, *3*, 1789–1795.
- (7) Walter, M. G.; Rudine, A. B.; Wamser, C. C. *J. Porphyrins Phthalocyanines* **2010**, *14*, 759–792.
- (8) Wu, S. L.; Lu, H. P.; Yu, H. T.; Chuang, S. H.; Chiu, C. L.; Lee, C. W.; Diao, E. W. G.; Yeh, C. Y. *Energy Environ. Sci.* **2010**, *3*, 949–955.
- (9) Lee, C. Y.; Hupp, J. T. *Langmuir* **2010**, *26*, 3760–3765.
- (10) Sugimoto, H.; Muto, M.; Tanaka, T.; Osuka, A. *Eur. J. Org. Chem.* **2011**, 71–77.
- (11) Maligaspe, E.; Kumpulainen, T.; Subbaiyan, N. K.; Zandler, M. E.; Lemmetyinen, H.; Tkachenko, N. V.; D'Souza, F. *Phys. Chem. Chem. Phys.* **2010**, *12*, 7434–7444.
- (12) Whited, M. T.; Djurovich, P. I.; Roberts, S. T.; Durrell, A. C.; Schlenker, C. W.; Bradforth, S. E.; Thompson, M. E. *J. Am. Chem. Soc.* **2011**, *133*, 88–96.
- (13) Tan, K.; Jaquinod, L.; Paolesse, R.; Nardis, S.; Di Natale, C.; Di Carlo, A.; Prodi, L.; Montalti, M.; Zaccheroni, N.; Smith, K. M. *Tetrahedron* **2004**, *60*, 1099–1106.
- (14) Koepf, M.; Trabolsi, A.; Elhabiri, M.; Wytko, J. A.; Paul, D.; Albrecht-Gary, A. M.; Weiss, J. *Org. Lett.* **2005**, *7*, 1279–1282.
- (15) Lee, C. Y.; Jang, J. K.; Kim, C. H.; Jung, J.; Park, B. K.; Park, J.; Choi, W.; Han, Y. K.; Joo, T.; Park, J. T. *Chem.—Eur. J.* **2010**, *16*, 5586–5599.
- (16) Loudet, A.; Burgess, K. *Chem. Rev.* **2007**, *107*, 4891–4932.
- (17) Liu, J.-Y.; El-Khouly, M. E.; Fukuzumi, S.; Ng, D. K. P. *Chem.—Eur. J.* **2011**, *17*, 1605–1613.
- (18) Jiao, C.; Zhu, L.; Wu, J. *Chem.—Eur. J.* **2011**, *17*, 6610–6614.
- (19) Lazarides, T.; Charalambidis, G.; Vuillamy, A.; Reglier, M.; Klontzas, E.; Froudakis, G.; Kuhri, S.; Guldi, D. M.; Coutsolelos, A. G. *Inorg. Chem.* **2011**, *50*, 8926–8936.
- (20) Benstead, M.; Mehl, G. H.; Boyle, R. W. *Tetrahedron* **2011**, *67*, 3573–3601.
- (21) Warnan, J.; Buchet, F.; Pellegrin, Y.; Blart, E.; Odobel, F. *Org. Lett.* **2011**, *13*, 3944–3947.
- (22) Sureshan, K. M.; Murakami, T.; Miyasou, T.; Watanabe, Y. *J. Am. Chem. Soc.* **2004**, *126*, 9174–9175.
- (23) Shiragami, T.; Tanaka, K.; Andou, Y.; Tsunami, S.; Matsumoto, J.; Luo, H. X.; Araki, Y.; Ito, O.; Inoue, H.; Yasuda, M. *J. Photochem. Photobiol., A* **2005**, *170*, 287–297.
- (24) Shiragami, T.; Matsumoto, J.; Inoue, H.; Yasuda, M. *J. Photochem. Photobiol., C* **2005**, *6*, 227–248.
- (25) Ermilov, E. A.; Liu, J. Y.; Ng, D. K. P.; Roder, B. *Phys. Chem. Chem. Phys.* **2009**, *11*, 6430–6440.
- (26) Liu, J. Y.; Ermilov, E. A.; Roder, B.; Ng, D. K. P. *Chem. Commun.* **2009**, 1517–1519.
- (27) Liu, J. Y.; Yeung, H. S.; Xu, W.; Li, X. Y.; Ng, D. K. P. *Org. Lett.* **2008**, *10*, 5421–5424.
- (28) Arnold, D. P. *J. Chem. Educ.* **1988**, *65*, 1111–1112.
- (29) Coskun, A.; Deniz, E.; Akkaya, E. U. *Org. Lett.* **2005**, *7*, 5187–5189.
- (30) Kolemen, S.; Bozdemir, O. A.; Cakmak, Y.; Barin, G.; Erten-Ela, S.; Marszalek, M.; Yum, J. H.; Zakeeruddin, S. M.; Nazeeruddin, M. K.; Gratzel, M.; Akkaya, E. U. *Chem. Sci.* **2011**, *2*, 949–954.
- (31) Smith, G.; Arnold, D. P.; Kennard, C. H. L.; Mak, T. C. W. *Polyhedron* **1991**, *10*, 509–516.
- (32) Altomare, A.; Cascarano, G.; Giacovazzo, C.; Guagliardi, A. J. *Appl. Crystallogr.* **1993**, *26*, 343–350.
- (33) Sheldrick, G. M. *Acta Crystallogr., A* **2008**, *64*, 112–122.
- (34) Demas, J. N.; Crosby, G. A. *J. Phys. Chem.* **1971**, *75*, 991–1024.
- (35) Casey, K. G.; Quitevis, E. L. *J. Phys. Chem.* **1988**, *92*, 6590–6594.
- (36) Seybold, P. G.; Gouterman, M. *J. Mol. Spectrosc.* **1969**, *31*, 1–13.
- (37) Du, H.; Fuh, R. C. A.; Li, J. Z.; Corkan, L. A.; Lindsey, J. S. *Photochem. Photobiol.* **1998**, *68*, 141–142.
- (38) Dixon, J. M.; Taniguchi, M.; Lindsey, J. S. *Photochem. Photobiol.* **2005**, *81*, 212–213.
- (39) Frisch, M. J. T., G. W.; Schlegel, H. B.; Scuseria, G. E.; Robb, M. A.; Cheeseman, J. R.; Montgomery, Jr., J. A.; Vreven, T.; Kudin, K. N.; Burant, J. C.; Millam, J. M.; Iyengar, S. S.; Tomasi, J.; Barone, V.; Mennucci, B.; Cossi, M.; Scalmani, G.; Rega, N.; Petersson, G. A.; Nakatsuji, H.; Hada, M.; Ehara, M.; Toyota, K.; Fukuda, R.; Hasegawa, J.; Ishida, M.; Nakajima, T.; Honda, Y.; Kitao, O.; Nakai, H.; Klene, M.; Li, X.; Knox, J. E.; Hratchian, H. P.; Cross, J. B.; Bakken, V.; Adamo, C.; Jaramillo, J.; Gomperts, R.; Stratmann, R. E.; Zazyev, O.; Austin, A. J.; Cammi, R.; Pomelli, C.; Ochterski, J. W.; Ayala, P. Y.; Morokuma, K.; Voth, G. A.; Salvador, P.; Dannenberg, J. J.; Zakrzewski, V. G.; Dapprich, S.; Daniels, A. D.; Strain, M. C.; Farkas, O.; Malick, D. K.; Rabuck, A. D.; Raghavachari, K.; Foresman, J. B.; Ortiz, J. V.; Cui, Q.; Baboul, A. G.; Clifford, S.; Cioslowski, J.; Stefanov, B. B.; Liu, G.; Liashenko, A.; Piskorz, P.; Komaromi, I.; Martin, R. L.; Fox, D. J.; Keith, T.; Al-Laham, M. A.; Peng, C. Y.; Nanayakkara, A.; Challacombe, M.; Gill, P. M. W.; Johnson, B.; Chen, W.; Wong, M. W.; Gonzalez, C.; Pople, J. A. *Gaussian03, RevisionD.01*; Gaussian: Wallingford, CT, 2004.
- (40) Becke, A. D. *Phys. Rev. A* **1988**, *38*, 3098–3100.
- (41) Lee, C. T.; Yang, W. T.; Parr, R. G. *Phys. Rev. B* **1988**, *37*, 785–789.
- (42) Cossi, M.; Barone, V.; Cammi, R.; Tomasi, J. *Chem. Phys. Lett.* **1996**, *255*, 327–335.
- (43) Takano, Y.; Houk, K. N. *J. Chem. Theory Comput.* **2005**, *1*, 70–77.
- (44) Tomasi, J.; Mennucci, B.; Cammi, R. *Chem. Rev.* **2005**, *105*, 2999–3093.
- (45) Arnold, D. P. *Polyhedron* **1986**, *5*, 1957–1963.
- (46) Arnold, D. P.; Blok, J. *Coord. Chem. Rev.* **2004**, *248*, 299–319.
- (47) Langford, S. J.; Lee, M. A. P.; Macfarlane, K. J.; Weigold, J. A. *J. Inclusion Phenom. Macrocycl. Chem.* **2001**, *41*, 135–139.
- (48) Giribabu, L.; Rao, T. A.; Maiya, B. G. *Inorg. Chem.* **1999**, *38*, 4971–4980.
- (49) Guenet, A.; Graf, E.; Kyritsakas, N.; Hosseini, M. W. *Inorg. Chem.* **2010**, *49*, 1872–1883.
- (50) Guenet, A.; Graf, E.; Kyritsakas, N.; Allouche, L.; Hosseini, M. W. *Chem. Commun.* **2007**, 2935–2937.
- (51) Lang, T.; Guenet, A.; Graf, E.; Kyritsakas, N.; Hosseini, M. W. *Chem. Commun.* **2010**, *46*, 3508–3510.
- (52) Burghart, A.; Kim, H. J.; Welch, M. B.; Thoresen, L. H.; Reibenspies, J.; Burgess, K.; Bergstrom, F.; Johansson, L. B. A. *J. Org. Chem.* **1999**, *64*, 7813–7819.
- (53) Lazarides, T.; McCormick, T. M.; Wilson, K. C.; Lee, S.; McCamant, D. W.; Eisenberg, R. J. *Am. Chem. Soc.* **2011**, *133*, 350–364.
- (54) Galletta, M.; Puntoriero, F.; Campagna, S.; Chiorboli, C.; Quesada, M.; Goeb, S.; Ziessel, R. *J. Phys. Chem. A* **2006**, *110*, 4348–4358.
- (55) Shetti, V. S.; Ravikanth, M. *J. Porphyrins Phthalocyanines* **2010**, *14*, 361–370.
- (56) Shetti, V. S.; Ravikanth, M. *Inorg. Chem.* **2010**, *49*, 2692–2700.
- (57) Arnold, D. P. *Polyhedron* **1988**, *7*, 2225–2227.
- (58) Ghiggino, K. P.; Hutchison, J. A.; Langford, S. J.; Latter, M. J.; Lee, M. A. P.; Lowenstern, P. R.; Scholes, C.; Takezaki, M.; Wilman, B. E. *Adv. Funct. Mater.* **2007**, *17*, 805–813.
- (59) Reddy, D. R.; Maiya, B. G. *J. Porphyrins Phthalocyanines* **2002**, *6*, 3–11.
- (60) Bullock, S. J.; Felton, C. E.; Fennessy, R. V.; Harding, L. P.; Andrews, M.; Pope, S. J. A.; Rice, C. R.; Riis-Johannessen, T. *Dalton Trans.* **2009**, 10570–10573.
- (61) Ventura, B.; Flamigni, L.; Beyler, M.; Heitz, V.; Sauvage, J. P. *Chem.—Eur. J.* **2010**, *16*, 8748–8756.
- (62) Flamigni, L.; Baranoff, E.; Collin, J. P.; Sauvage, J. P. *Chem.—Eur. J.* **2006**, *12*, 6592–6606.

(63) Transient absorption measurements on **3** and **6** show no evidence of thermal equilibrium between the triplet excited states of the Bodipy and porphyrin chromophores. This could be due to the dominant spectral features of the Sn(IV) porphyrin triplet excited state which would mask those of the Bodipy.

(64) Ou, Z. P.; E, W. B.; Zhu, W. H.; Thordarson, P.; Santic, P. J.; Crossley, M. J.; Kadish, K. M. *Inorg. Chem.* **2007**, *46*, 10840–10849.

(65) Maeda, D.; Shimakoshi, H.; Abe, M.; Fujitsuka, M.; Majima, T.; Hisaeda, Y. *Inorg. Chem.* **2010**, *49*, 2872–2880.

(66) Gnichwitz, J. F.; Wielopolski, M.; Hartnagel, K.; Hartnagel, U.; Guldi, D. M.; Hirsch, A. *J. Am. Chem. Soc.* **2008**, *130*, 8491–8501.

(67) Berho, F.; Lesclaux, R. *Chem. Phys. Lett.* **1997**, *279*, 289–296.

(68) Li, C.; Hoffman, M. Z. *J. Phys. Chem. B* **1999**, *103*, 6653–6656.

(69) Sabatini, R. P.; McCormick, T. M.; Lazarides, T.; Wilson, K. C.; Eisenberg, R.; McCamant, D. W. *J. Phys. Chem. Lett.* **2011**, *2*, 223–227.

(70) Lakowicz, J. R. *Principles of Fluorescence Spectroscopy*, 2nd ed.; Kluwer/Plenum: New York, 1999.

(71) Förster, T. *Ann. Phys.* **1948**, *437*, 55–75.

(72) Förster, T. *Discuss. Faraday Soc.* **1959**, *27*, 7–17.

(73) Dexter, D. L. *J. Chem. Phys.* **1953**, *21*, 836–850.

(74) Lazarides, T.; Sykes, D.; Faulkner, S.; Barbieri, A.; Ward, M. D. *Chem.—Eur. J.* **2008**, *14*, 9389–9399.

(75) Keyes, T. E.; Leane, D.; Forster, R. J.; Coates, C. G.; McGarvey, J. J.; Nieuwenhuyzen, M. N.; Figgemeier, E.; Vos, J. G. *Inorg. Chem.* **2002**, *41*, 5721–5732.

(76) Weinstein, J. A.; Tierney, M. T.; Davies, E. S.; Base, K.; Robeiro, A. A.; Grinstaff, M. W. *Inorg. Chem.* **2006**, *45*, 4544–4555.

(77) Prieto, J. B.; Arbeloa, F. L.; Martinez, V. M.; Lopez, T. A.; Arbeloa, I. L. *Phys. Chem. Chem. Phys.* **2004**, *6*, 4247–4253.